03,08

Influence of oxygen and substrate temperature on the electrical properties of ZnO thin films deposited by ion-beam sputtering

© V.A. Makagonov, K.S. Gabriels, Yu.E. Kalinin, A.Yu. Lopatin, V.A. Okorochkov

Voronezh State Technical University,
Voronezh, Russia

E-mail: lopatin-ayu@mail.ru

Received October 29, 2025
Revised December 7, 2025
Accepted December 10, 2025

The influence of the reactive gas (oxygen) partial pressure in the deposition chamber and the substrate temperature on the electrical conductivity, charge carrier mobility, and thermoelectric power of zinc oxide (ZnO) thin films obtained by ion-beam sputtering has been studied. The synthesized films are nanocrystalline and are characterized by a wurtzite hexagonal crystal lattice and a texture with a predominant $\langle 0001 \rangle$ axis perpendicular to the film plane. Electron microscopic analysis confirmed the formation of a nanocrystalline structure with a characteristic growth texture.

It has been established that the dominant charge transport mechanism in the studied samples is variable-range hopping conduction through localized states near the Fermi level, as confirmed by the linearity of the $\ln(\rho/\rho_o)(T^{-1/4})$ and $S(T^{1/2})$ dependences, as well as by the low values of the density of localized states at the Fermi level $g(E_F) \sim 10^{17}\,\mathrm{eV}^{-1}\cdot\mathrm{cm}^{-3}$. Estimates of the main model parameters of the studied films were carried out: the characteristic temperature B, the density of states at the Fermi level $g(E_F)$, the hopping length, and the localization radius. It was found that an increase in the oxygen partial pressure in the gas mixture leads to a decrease in $g(E_F)$, while an increase in the substrate temperature promotes the growth of the density of electronic states.

Keywords: zinc oxide, electrical properties, thermoelectric power, density of electronic states.

DOI: 10.61011/PSS.2025.12.63077.304-25

1. Introduction

Zinc oxide (ZnO) continues to arouse increased interest among researchers due to a number of significant advantages. Zinc oxide has a record exciton binding energy of -60 meV among binary semiconductors, which is a prerequisite for creating devices that operate efficiently at temperatures up to 700 °C [1] and has a wide band gap (~ 3.37 eV) and stability in aggressive environments [2]. In addition, ZnO is susceptible to chemical etching, harmless and relatively inexpensive, which makes it attractive for creating a wide variety of electronic devices [3]. From a practical point of view, zinc oxide is a promising material for electrodes of transparent electronics, sensitive layers of gas and biological sensors, catalysts, X-ray and γ-radiation detectors [4–6], as well as other applications [7,8]

It is known that the electrical conductivity of zinc oxide films significantly depends on the conditions of their synthesis [9]. At the same time, the values of electrical conductivity presented in the literature vary from those typical for degenerate semiconductors with a band conduction mechanism to very small ones typical for insulators with activation or hopping conductivity [10]. This indicates that at a certain level of defects in zinc oxide films, localization of mobile charge carriers may occur. At the same time, the mechanisms of this localization and the parameters of localized electronic states remain poorly understood, while their understanding is important for obtaining films with higher electron mobility and developing a technology for their synthesis.

Various methods are used to produce zinc oxide films: molecular beam epitaxy [11], magnetron sputtering [12], vapor-phase deposit [13], including organometallic and pulsed laser spraying [14], as well as others [15,16]. However, the quality of ZnO thin films obtained by physical or chemical deposition significantly depends on the synthesis parameters, including substrate temperature, pressure, and gas composition. The role of oxygen is especially important, which affects the stoichiometry of the material, the concentration of defects and, as a result, its electronic and optical characteristics [17]. The lack of oxygen leads to the formation of oxygen vacancies (V_O) and interstitial zinc atoms (Zn_i), which increases the density of localized states in the band gap and reduces the mobility of charge carriers. On the contrary, excess oxygen can cause the formation of surface oxides or secondary phases that disrupt the crystal structure [18]. Modern research shows that optimizing the oxygen content in the synthesis chamber makes it possible to improve the structural perfection of ZnO films and control their electrical properties. For example, when using reactive magnetron sputtering with a controlled oxygen flow, high crystalline purity and uniformity of films are achieved [19].

The relevance of this study is attributable to the need to establish quantitative patterns between the oxygen con-

tent during synthesis, the substrate temperature, and the electronic structure of ZnO films. Solving this problem will make it possible to create materials with specified characteristics for applications in transistors, solar cells, resistive random-access memory (RRAM) cells and gas sensors. Preliminary studies have shown that for zinc oxide films obtained by ion beam sputtering, despite their crystalline structure, at temperatures above room temperature, a hopping conduction mechanism is implemented in localized states near the Fermi level with a variable hopping length. Using the already developed technique, it was possible to experimentally determine the density of localized states and its change depending on the technological parameters of film deposition from the results of temperature dependences of electrical conductivity. With this in mind, the aim of the paper was to study the dependence of the density of electronic states on the temperature of the substrate for samples synthesized at various oxygen concentrations, followed by an analysis of the mechanisms of defect formation and their effect on conductivity. To achieve this goal, the method of ion beam sputtering in a controlled atmosphere was used, as well as comprehensive studies of structural and electronic properties, including X-ray diffraction [20].

2. Experimental methodology

To obtain experimental samples, the ion beam sputtering method was used, implemented on the basis of the UVN-2M vacuum station, the device of which is described in detail in the work [21]. CT-50 polycrystalline glass (samples for measuring electrical properties and the Hall effect) and oxidized silicon (for studying the structure) orientation (001) were used as substrates. A water-cooled target consisting of ZnO ceramic plates was used to produce thin films. Deposition was performed on a heated substrate, the temperature of which was maintained at $T_{\text{sub}} = 200, 300, 400, 500\,^\circ\text{C}$ for various sprays. The gas atmosphere in the sputtering chamber was created as follows: the pre-working volume was evacuated to the pressure of residual gases of 10^{-7} Torr, then the working gas — 99.9995 % argon was admitted through software-controlled leak valves to the pressure of $7 \cdot 10^{-4}$ Torr and 99.9999 % oxygen ranging from 0 to 10 % of the working one. The substrates were positioned vertically on a substrate holder, which moves them to the spray zones or ion purification zone at a set speed. Ion cleaning of the substrates was performed for 5 min before applying the film. The operating parameters of ion sources: accelerating voltage 2.0 kV, plasma current 60 mA. The application rate of the material was $\sim 0.5\,\mu$m per hour. The thickness of the obtained films was measured using MII-4 interferometer and was $\sim 0.8\,\mu$m.

X-ray diffraction phase analysis (XRD) and transmission electron microscopy (TEM) techniques were used to study the structure and phase composition of the obtained samples. X-ray diffraction was performed using Bruker D2 Phaser diffractometer ($\lambda_{\text{Cu}K\alpha1} = 1.54\,\text{Å}$) with DIFFRAC.EVA 3.0 software and the ICDD PDF Release 2012 database [22].

The study of the electrical conductivity and thermo-emf of the obtained samples was carried out using a differential method on a Netzsch SBA458 system in the temperature range of 300−550 K [23]. Rectangular samples with sides 20×4 mm were used to perform these measurements.

The Hall coefficient was measured by the Van der Pau method on an Ecopia HMS-5500 installation. This measuring system allows for automatic recording of the values of mobility, volume and surface concentrations of charge carriers and the Hall coefficient [24]. The measurement was performed in a constant magnetic field of 0.55 T on samples in the form of a square with a side length of 10 mm, the corners of which were previously coated with ohmic contacts made of PP-17 paste.

3. Results and their discussion

3.1. Structure of ZnO thin films

The results of XRD of ZnO thin films are shown in Figure 1. Analysis of the diffractograms showed that all the samples studied were characterized by the crystalline structure of zinc oxide with a hexagonal wurtzite lattice (spatial group $P63mc$). When up to and including 10 % of oxygen is added the films are predominantly textured with the texture axis $\langle 0001 \rangle$ perpendicular to the film plane, which manifests itself as an increase in intensity from the reflex (0002) relative to the reference value of the card PDF 01-089-1397 of the ICDD PDF 2012 database. The evaluation of the unit cell parameters gave the values $a = 3.36 \pm 0.02\,\text{Å}$ and $c = 5.24 \pm 0.02\,\text{Å}$, which are practically independent of the substrate temperature and oxygen pressure. Comparing the obtained values with the tabular parameters ($a = 3.325\,\text{Å}$ and $c = 5.205\,\text{Å}$), it can be concluded that thin films of crystalline ZnO with a defective structure are formed during ion beam sputtering on a fixed substrate, which leads to an increase in the parameters a and c. Estimation of crystallite sizes using the Scherrer formula

$$d = \frac{K\lambda}{\beta \cos\theta}, \tag{1}$$

where d is the average crystal size, K is the dimensionless particle shape coefficient, λ is the X-ray wavelength, β is the width half-height reflection (in radians), θ is the diffraction angle (Bragg angle), gives sufficiently large values ~ 28 nm. The addition of oxygen does not lead to the appearance of new phases or a significant change in the unit cell parameters.

An increase in the intensity and decrease in the broadening of ZnO diffraction peaks observed for diffractograms at $T_{\text{sub}} = 400\,^\circ\text{C}$ (Figure 1, *b*) in comparison with $T_{\text{sub}} = 200\,^\circ\text{C}$ (Figure 1, *a*) indicate an improvement in the

structural perfection of films deposited at elevated temperatures and a larger crystallite size than at $T_{sub} = 200\,^\circ$C. This effect is evident in the entire studied range of partial oxygen concentrations ($n_{O2} = 1-10\,\%$). The main reason for the observed improvement is the thermal activation of processes on the substrate surface: an increase in temperature to $400\,^\circ$C enhances the surface diffusion of adsorbed atoms and the processes of lattice rearrangement (recrystallization), which contributes to the formation of larger ZnO crystallites. For samples synthesized at $T_{sub} = 400\,^\circ$C, estimates of crystallite sizes gave values of ~ 38 nm.

An analysis of a TEM micrograph of a cross-section of a thin ZnO film obtained without adding oxygen to a substrate at $T_{sub} = 200\,^\circ$C (Figure 2) showed that the structure of the studied sample is nanocrystalline and characterized by a hexagonal ZnO phase of the wurtzite type, as indicated by the presence of arc-shaped reflections in the electron diffraction patterns (inset in Figure 2). Based on the analysis of electron diffraction patterns, it can also be concluded

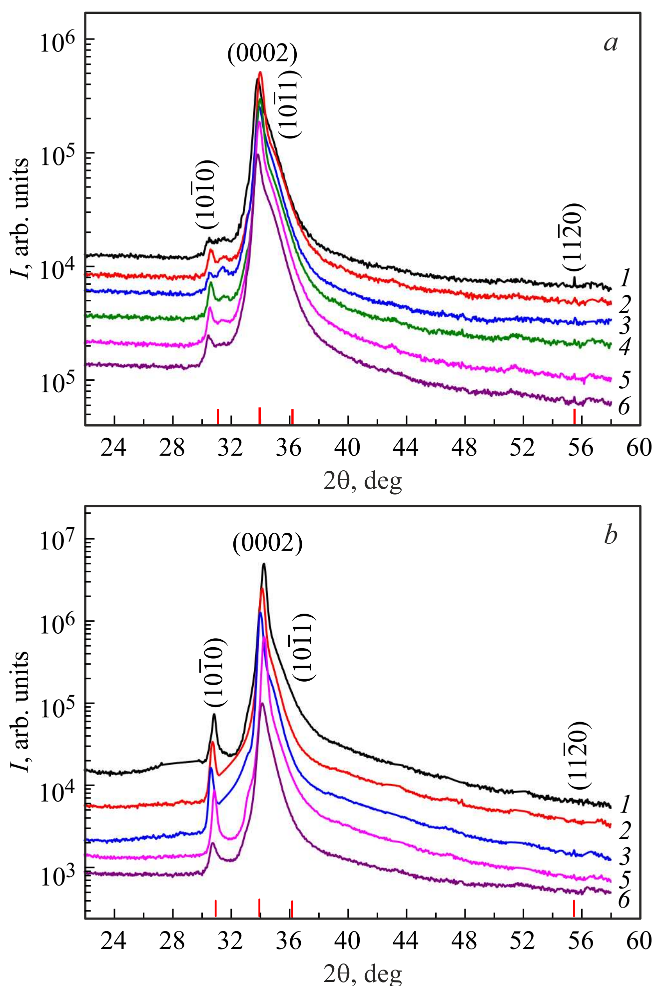

Figure 1. X-ray diffractograms ($\lambda_{\mathrm{Cu}K\alpha 1} = 1.54$ Å) of thin ZnO films deposited on substrates at $T_{sub} = 200\,^\circ$C (a) and $T_{sub} = 400\,^\circ$C (b): *1* — $n_{O2} = 1\,\%$, *2* — $n_{O2} = 1.2\,\%$, *3* — $n_{O2} = 1.4\,\%$, *4* — $n_{O2} = 2.4\,\%$, *5* — $n_{O2} = 5\,\%$, *6* — $n_{O2} = 10\,\%$.

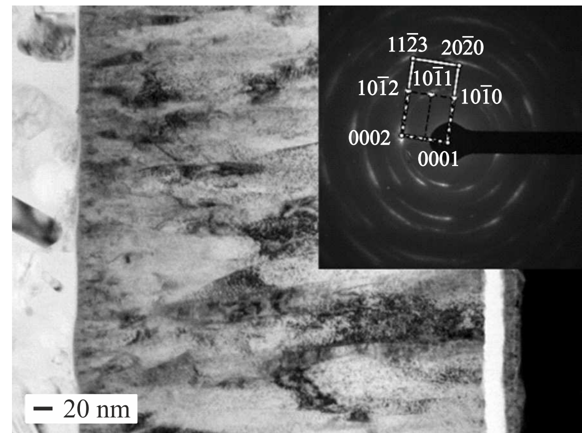

Figure 2. TEM image of the cross-section and electron diffraction pattern (on the insert) of thin ZnO films obtained without adding oxygen to the substrate at $T_{sub} = 200^\circ$ C.

that the studied thin films contain ZnO crystallites of two orientations determined by the selective grain growth with an axis of $\langle 0001 \rangle$, the normal surface of the substrate. The mutual orientation of ZnO grains is described by the ratio $(10\bar{1}0)$, $[0001] \parallel (11\bar{2}0)$, $[0001]$ (the plane $(10\bar{1}0)$ and the direction $[0001]$ of some crystallites are parallel to the plane $(11\bar{2}0)$ and the direction $[0001]$ of other crystallites).

It should be noted that there is some misorientation of the crystallites relative to the $\langle 0001 \rangle$ axis, which manifests itself in electron diffraction as an arc-shaped blurring of reflexes.

3.2. Electrical properties of zinc oxide thin films

The results of measurements of the dependences of electrical resistivity on the temperature of synthesized thin films of zinc oxide are shown in Figure 3. It can be seen from Figure 3, a that the values of electrical resistivity for all the studied films decrease with an increase in temperature to 500 K. At room temperature, the magnitude of the electrical resistance significantly depends on the partial pressure of oxygen in the sputtering chamber: an increase in the partial pressure from 0 to 10 % leads to an increase in electrical resistance by several orders of magnitude (Figure 3, a).

To establish the dominant conduction mechanism, the experimental dependences $\rho(T)$, shown in Figure 3, a, were rearranged in coordinates $\ln(\rho/\rho_o)(1/T)$, $\ln(\rho/\rho_o)(1/T^{1/2})$, $\ln(\rho/\rho_o)(1/T^{1/4})$ (where ρ_o is the electrical resistance at room temperature), and it was found that the electrical resistivity has a linear dependence in coordinates $\ln(\rho/\rho_o)(1/T^{1/4})$ in the temperature range of 300–500 K (Figure 3, b). The dependences shown in Figure 3, b indicate a hopping mechanism for the conduction of charge carriers with a variable hopping length over localized states lying in a narrow energy band near the Fermi level. It should be noted that the linear dependence $\rho(T)$ for an iron-doped ceramic sample of zinc oxide in Mott coordinates was observed in the temperature range of $20\,\mathrm{K} < T < 40\,\mathrm{K}$ [25].

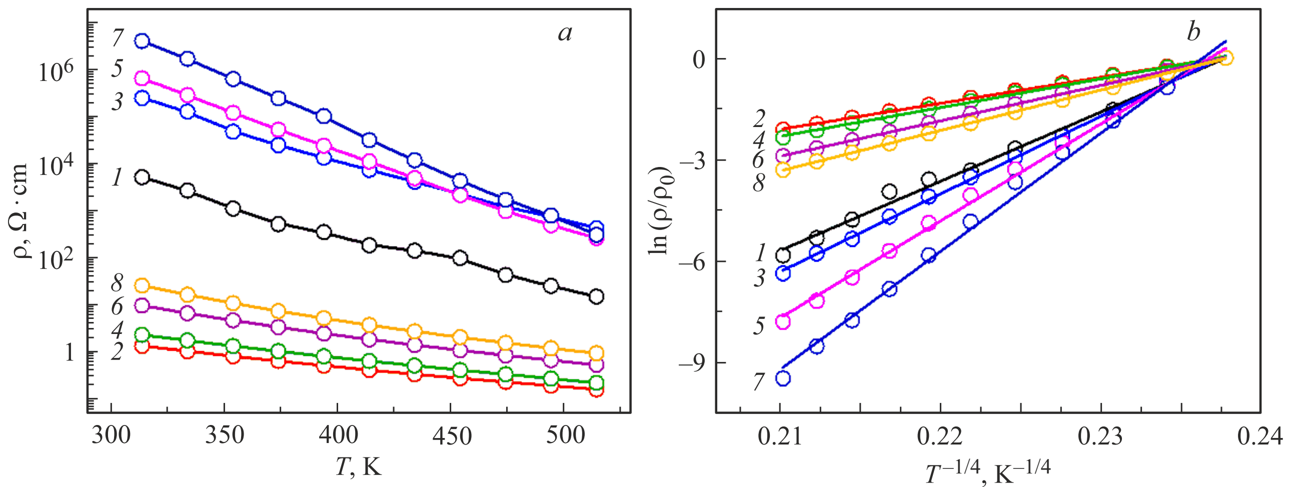

Figure 3. Dependencies $\rho(T)$ (a) and $\ln(\rho/\rho_o)(T^{-1/4})$ (b) for thin films of zinc oxide sprayed at $T_{sub} = 200\,^\circ$C (*1, 3, 5, 7*) and $T_{sub} = 400\,^\circ$C (*2, 4, 6, 8*) with different oxygen content in the chamber: *1, 2* — $n_{O2} = 0\,\%$; *3, 4* — $n_{O2} = 1.4\,\%$; *5, 6* — $n_{O2} = 5\,\%$; *7, 8* — $n_{O2} = 10\,\%$.

In the case of a thin-film unalloyed zinc oxide sample with a nanocrystalline structure obtained by the ion beam method in this work, when a high concentration of broken chemical bonds is formed along the grain boundaries due to the lack of oxygen stoichiometry, the hopping conduction mechanism is realized at temperatures above room temperature.

The equation [26] is valid for the hopping conductivity of electrons with variable hopping length in localized states near the Fermi level:

$$\sigma = e^2 \cdot R^2 \cdot \nu_{ph} \cdot g(E_F) \cdot \exp\left(-\frac{B}{T}\right)^{1/4}, \tag{2}$$

where

$$B = \frac{21}{a^3 \cdot k_B \cdot g(E_F)}, \tag{3}$$

$$K = \left(\frac{3 \cdot a}{2\pi \cdot g(E_F) \cdot k_B \cdot T}\right)^{1/4}, \tag{4}$$

e is the electron charge, K is the average hopping length, ν_{ph} is the phonon interaction spectrum factor, T is the absolute temperature, $g(E_F)$ is the density of states at the Fermi level, a is the radius of localization of the electron wave function, k_B is the Boltzmann constant.

The values of B for the studied films were determined from Figure 3, *b*. Assuming that the process of charge carrier transfer is limited by hops between dangling bonds along the boundaries of crystallites, to estimate the density of localized states, we assume a localization radius equal to the Bohr radius [27]:

$$a = a_B = \frac{4\pi\varepsilon_0\varepsilon\hbar^2}{m^* e^2}, \tag{5}$$

where ε_0 is the electrical constant, $\varepsilon = 9$ is the static permittivity of ZnO [28], $\hbar$ is the reduced Planck constant, $m^* \approx 0.24 m_0$ is the effective electron mass for ZnO [28.29], m_0 is the electron rest mass, e is the electron charge, which gives $a_B = 2$ nm.

Then, using expressions (2)–(5), it is possible to estimate the parameters of a thin zinc oxide film according to the model of hopping conduction of electrons with a variable hopping length for localized states lying in a narrow energy band near the Fermi level, the density of electronic states from equation (2), and also, the hopping length K and the average hopping energy W_{VRH} can be estimated according to the formula:

$$W_{VRH} \cong \frac{1}{4} k_B T \left(\frac{B^4}{T}\right)^{1/4}, \tag{6}$$

where k_B is the Boltzmann constant, T is the absolute temperature, B is the parameter in equation (2).

The densities of localized states at the Fermi level of thin-film zinc oxide were determined according to experimental data on Figure 3, *b* from the equation (3) (see Table) and are shown in Figure 4 as dependences $g(E_F)$ on the partial pressure O_2 in the chamber in case of sputtering (Figure 4, *a*) and on the substrate temperature (Figure 4, *b*). The results of the calculation of other parameters are also shown in the table.

With an increase in partial pressure O_2, a monotonous decrease of $g(E_F)$ is observed in the spray chamber (Figure 4, *a*) as for $T_{sub} = 200\,^\circ$C and for $T_{sub} = 400\,^\circ$C, which is probably due to a decrease in the concentration of oxygen vacancies. At the same time, at low substrate temperatures, the effect is more pronounced: at $T_{sub} = 200\,^\circ$C $g(E_F)$ decreases by two orders of magnitude with increasing partial pressure O_2 in the sputtering chamber.

Figure 4, *b* shows the dependence of $g(E_F)$ on T_{sub} at different concentrations O_2 in the chamber during sputtering. It can be seen from Figures 4, *a* and *b* that the density of localized states at the Fermi level increases with

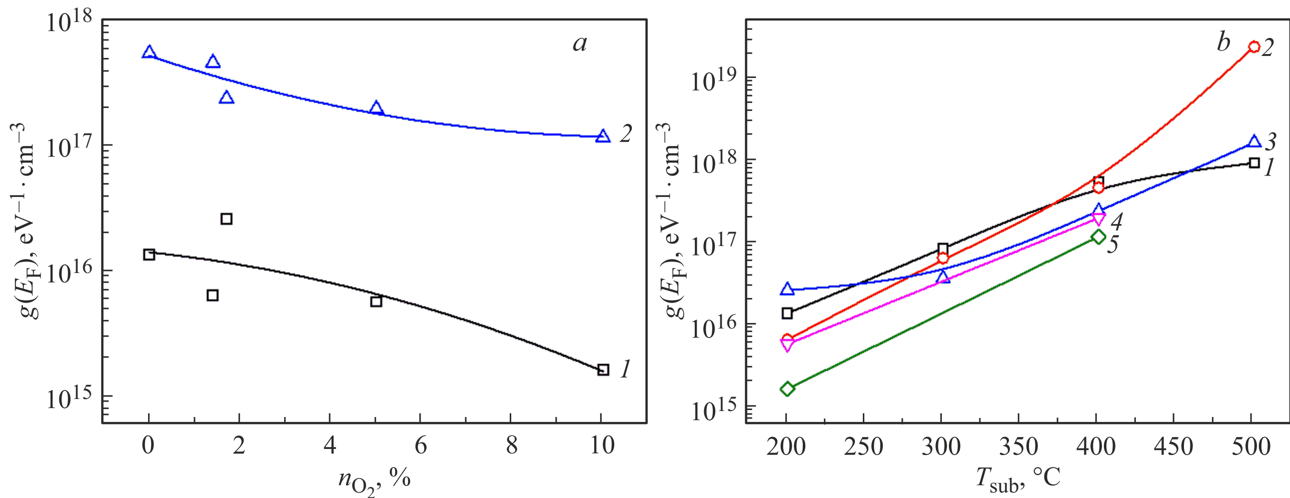

Figure 4. Dependences $g(E_F)$ on the concentration O_2 (n_{O2}) in the chamber during sputtering (*a*), where *1* —$T_{sub} = 200\,^\circ$C, *2* — $T_{sub} = 400\,^\circ$C and the substrate temperature (*b*), where *1* — $n_{O2} = 0\,\%$, *2* — $n_{O2} = 1.4\,\%$, *3* — $n_{O2} = 1.7\,\%$, *4* — $n_{O2} = 5\,\%$, *5* — $n_{O2} = 10\,\%$.

Parameters of ZnO thin films calculated according to the model of hopping conduction of electrons with a variable hopping length for localized states lying in a narrow energy band near the Fermi level

Atmosphere in case of sputtering	T_{sub}, °C	n_{O_2}, %	$B^{1/4}$, K$^{1/4}$	$g(E_F)$, eV^{-1} · cm^{-3}	K, nm ($T = 300$ K)	W_{VRH}, eV ($T = 300$ K)	$\left(\frac{\partial \ln\left(\frac{g(E_F)}{g_0}\right)}{\partial E}\right)_{E=E_F}$, eV^{-1} ($T = 300$ K)
Ar	200	–	204.1	$1.3 \cdot 10^{16}$	40.8	0.32	−0.024
	300	–	130.1	$8.1 \cdot 10^{16}$	26.0	0.21	–
	400	–	81.3	$5.3 \cdot 10^{17}$	16.2	0.13	−0.238
	500	–	71.4	$8.9 \cdot 10^{17}$	14.3	0.11	–
Ar+O_2	200	1.4	245.5	$6.4 \cdot 10^{15}$	49.0	0.38	−0.016
	300		138.8	$6.2 \cdot 10^{16}$	27.7	0.22	–
	400		84.8	$4.5 \cdot 10^{17}$	16.9	0.13	−0.220
	500		31.7	$2.3 \cdot 10^{19}$	6.3	0.05	–
	200	1.7	173.6	$2.6 \cdot 10^{16}$	34.7	0.27	−0.032
	300		159.7	$3.6 \cdot 10^{16}$	31.9	0.24	–
	400		100.1	$2.3 \cdot 10^{17}$	20.0	0.25	−0.173
	500		61.9	$1.6 \cdot 10^{18}$	12.4	0.16	–
	200	5	253.2	$5.6 \cdot 10^{15}$	50.6	0.39	−0.023
	400		104.8	$1.9 \cdot 10^{17}$	20.9	0.16	−0.189
	200	10	346.1	$1.6 \cdot 10^{15}$	69.1	0.54	−0.029
	400		119.4	$1.1 \cdot 10^{17}$	23.9	0.19	−0.210

increasing substrate temperature. This may be attributable to the fact that the interaction of oxygen with zinc during film synthesis occurs on the surface of the substrate, and as its temperature increases, oxygen atoms desorb, which leads to the formation of oxygen vacancies and an increase in the density of localized states associated with them.

Thus, an increase in the partial pressure of oxygen in the sputtering chamber during the growth of the zinc oxide film and a change in the substrate temperature make it possible to change the density of localized states in thin zinc oxide films over a wide range (by several orders of magnitude) and control the electrical properties of the formed films.

As noted in the introduction, the hopping conduction mechanism, implemented with a lack of oxygen in the film, should have an effect on reducing the mobility of charge carriers, for which the temperature dependences of electron mobility, defined as the product of electrical conductivity by the Hall coefficient, were investigated. Figure 5, *a* shows the temperature dependence of charge carrier mobility for synthesized zinc oxide samples. It can be seen from Figure 5, *a* that the observed values at room temperature have values characteristic of hopping conductivity, and the mobility increases with increase of the temperature for all the samples studied in the paper. This behavior distinguishes

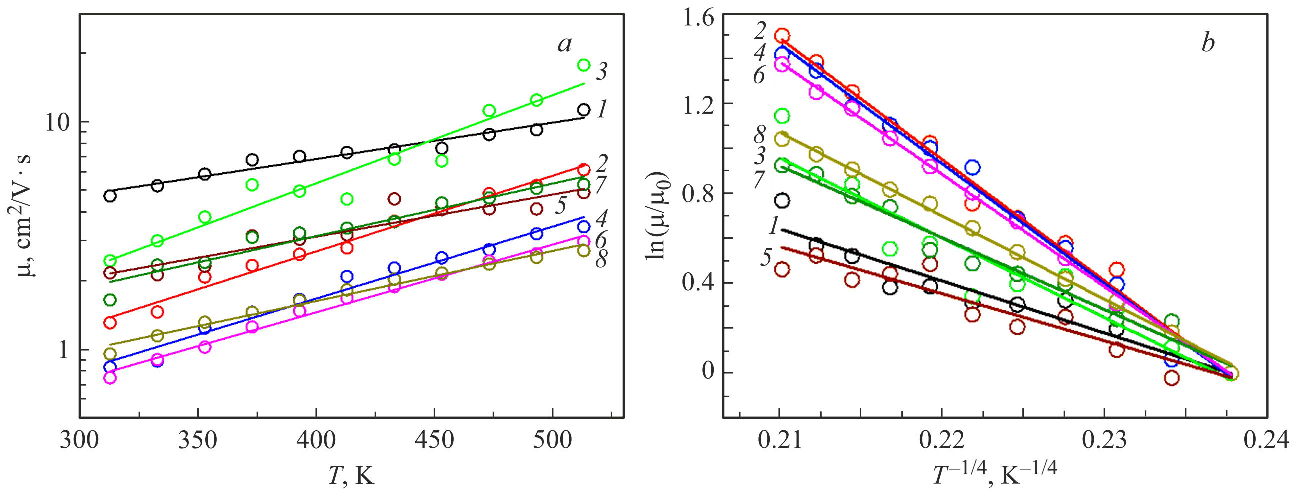

Figure 5. Dependencies $\mu(T)$ (*a*) and $\ln(\mu/\mu_o)(T^{-1/4})$ (*b*) for thin films of zinc oxide sprayed at $T_{\text{sub}} = 200\,^\circ\text{C}$ (*1, 3, 5, 7*) and $T_{\text{sub}} = 400\,^\circ\text{C}$ (*2, 4, 6, 8*) with different oxygen content in the chamber: *1, 2* — $n_{\text{O2}} = 0\,\%$; *3, 4* — $n_{\text{O2}} = 1.4\,\%$; *5, 6* — $n_{\text{O2}} = 5\,\%$; *7, 8* — $n_{\text{O2}} = 10\,\%$.

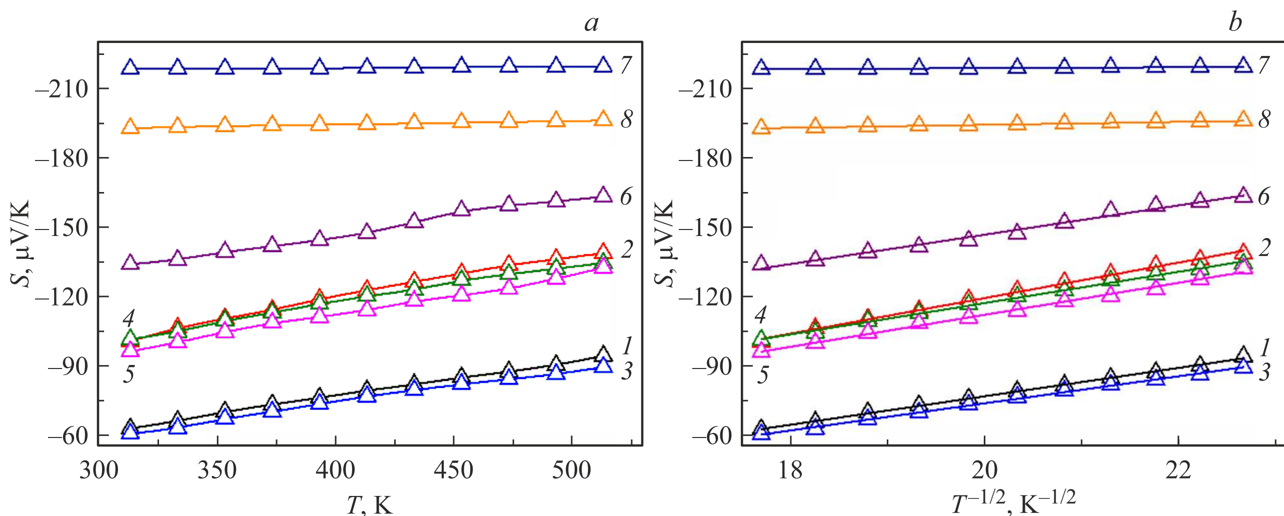

Figure 6. Dependencies $S(T)$ (*a*) and $S(T^{1/2})$ (*b*) for zinc oxide films deposited at $T_{\text{sub}} = 200\,^\circ\text{C}$ (*1, 3, 5, 7*) and $T_{\text{sub}} = 400\,^\circ\text{C}$ (*2, 4, 6, 8*) with different oxygen content in the chamber: *1, 2* — $n_{\text{O2}} = 0\,\%$; *3, 4* — $n_{\text{O2}} = 1.4\,\%$; *5, 6* — $n_{\text{O2}} = 5\,\%$; *7, 8* — $n_{\text{O2}} = 10\,\%$.

the films under study from conventional semiconductors, in which mobility decreases at temperatures above room temperature due to increased scattering by thermal lattice vibrations.

Figure 5, *b* shows the mobility dependences in Mott coordinates $\ln(\mu/\mu_o)(1/T^{1/4})$, where μ_o are the mobility values of charge carriers at room temperature. The observed linear dependences indicate that mobility increases with increasing temperature according to the law characteristic of hopping conduction with variable hopping length. Thus, the mobility analysis independently and unambiguously confirms the conclusion about the dominance of the hopping conduction mechanism in the obtained zinc oxide films.

An experimental study of thermo-emf in semiconductor films allows us to obtain additional information about the mechanisms of electron transfer, for which ZnO is used in synthesized films. The temperature dependences of thermo-emf were studied, the measurement results of which are shown in Figure 6, *a*. At room temperature, for films synthesized in an argon atmosphere, the thermo-emf value is relatively small ($S \sim 60\,\mu$V/K) and increases slightly with increasing temperature (curves *1* and *2* in Figure 6, *a*). An increase in the partial pressure of oxygen in the sputtering chamber to 10 % leads to an increase in thermo-emf to $S \sim 220\,\mu$V/K at room temperature (curve *7* in Figure 6, *a*). It should be noted that the thermo-emf sign is negative for all synthesized samples, which indicates the electronic type of charge carriers.

If there is a hopping conduction mechanism in the studied temperature range with a variable hopping length over

localized states lying in a narrow energy band near the Fermi level, then the following expression should be valid for thermo-emf [30]:

$$S = \frac{k_B}{2e}\sqrt{BT}\left(\frac{\partial \ln(\frac{g(E_F)}{g_0})}{\partial E}\right)_{E=E_F}, \quad (7)$$

where k_B is the Boltzmann constant, e is the electron charge, T is the absolute temperature, B is the parameter in equation (2), $\left(\frac{\partial \ln(\frac{g(E_F)}{g_0})}{\partial E}\right)_{E=E_F}$ is the energy derivative of the logarithm of the density of localized states at the Fermi level.

By reconstructing the experimental dependences of thermo-emf in coordinates $S(T^{1/2})$, it is possible to see that the measured samples show a linear relationship (Figure 6, b). These dependences confirm that hopping conduction in localized states near the Fermi level prevails in the studied temperature range. Taking into account the previously obtained values of B and S, it is possible to estimate the values of the logarithm derivative of the density of localized states at the Fermi energy level for various temperatures. The results of such tests for the studied samples are presented in the table.

In conclusion, we note that by changing such conditions for the synthesis of thin zinc oxide films as the substrate temperature and oxygen partial pressure, it is possible to control the concentration of oxygen vacancies, thus changing the density of localized states at the Fermi level and obtaining specified electrical properties.

4. Conclusion

The electrophysical properties of thin zinc oxide (ZnO) films obtained by ion beam sputtering at various oxygen partial pressure values in the sputtering chamber and substrate temperatures have been studied. The synthesized films are nanocrystalline and are characterized by a hexagonal crystal lattice and a texture with a predominant axis $\langle 0001 \rangle$ perpendicular to the film plane.

An analysis of the temperature dependences of electrical conductivity and thermo-emf showed that the hopping conductivity with a variable hopping length near the Fermi level is the predominant charge transfer mechanism in the studied samples in the temperature range of 300−500 K. This is confirmed by the linearity of the dependencies $\ln(\rho/\rho_o)(T^{-1/4})$ and $S(T^{1/2})$, as well as low values of the density of states at the Fermi level $g(E_F) \sim 10^{17}\,\mathrm{eV}^{-1}\cdot\mathrm{cm}^{-3}$, typical for localized states. The main model parameters of the studied ZnO films were calculated: the characteristic temperature B, the density of states at the Fermi level $g(E_F)$, the hopping length and the localization radius. It has been found that an increase in the partial pressure of oxygen in a gas mixture leads to a decrease in $g(E_F)$, and an increase in the temperature of the substrate contributes to an increase in the density of electronic states.

Funding

This study was supported by the Russian Science Foundation (grant No. 24-29-20099).

Conflict of interest

The authors declare that they have no conflict of interest.

References

[1] R. Ismail, M.T. Ahmadi, S. Anwar. Advanced Nanoelectronics. CRC Press, Boca Raton, FL (2013). 456 p.
[2] Q. Zhang, F. Li, X. Chang, D. He. Mater. Manuf. Process. **29**, 789 (2014).
[3] L.V. Grigoriev, A.A. Semenov, A.V. Mikhailov. FTP **55**, *12*, 1180 (2021) (in Russian).
[4] D. Tainoff, B. Masenelli, O. Boisron, G. Guiraud, P. Mélinon. J. Phys. Chem. C **112**, *33*, 12623 (2008).
[5] K. Ellmer. Transparent Conductive Zinc Oxide and Its Derivatives. Springer, N.-Y. (2010). P. 193.
[6] N.V. Lyanguzov. Sintez nanostruktur na osnove oksida cinka i ih fizicheskie svojstva: avtoref. kand. diss. (Rostov on Don (2014) (in Russian).
[7] O.A. Novodvorsky, L.S. Gorbatenko, V.Ya. Panchenko, O.D. Khramova, E.A. Cherebylo, K. Ventsel, J.V. Barta, V.T. Bublik, K.D. Shcherbachev. FTP **43**, *4*, 439 (2009) (in Russian).
[8] N.A. Lashkova, A.I. Maksimov, A.A. Ryabko, A.A. Bobkov, V.A. Moshnikov, E.I. Terukov. FTP **50**, *9*, 1276 (2016) (in Russian).
[9] S.I. Rembeza, N.N. Kosheleva, E.S. Rembeza, T.V. Svistova, A.A. Vinokurov. Lett. Mater. **10**, *4*, 469 (2020).
[10] S.I. Rembeza, E.S. Rembeza, T.V. Svistova, N.N. Kosheleva. Sintez i svojstva metallooksidnyh plenok: monografiya. VGTU, Voronezh, (2017) (in Russian).
[11] Y. W.Heo, D.P. Norton, S.J. Pearton. J. Appl. Phys. **98**, 073502 (2005).
[12] S. Besleaga, G.E. Stan, A.C. Galka, L. Ion, S. Antohe. Appl. Surf. Sci. **258**, *22*, 8819 (2012).
[13] V.S. Burakov, N.V. Tarasenko, E.A. Nevar, M.I. Nedelko. ZhTF **81**, *2*, 89 (2011) (in Russian).
[14] J.L. Zhao, X.M. Li, J.M. Bian. J. Cryst. Growth **276**, 507 (2005).
[15] D. Fang, K. Lin, T. Xue, C. Cui. J. Alloys Compd. **589**, 346 (2014).
[16] D. Kim, H. Kim, I. Yun. Curr. Appl. Phys. **10**, *3*, 459 (2010).
[17] A.E. Muslimov, M.Kh. Rabadanov, A.M. Ismailov. Prikl fiz. **3**, 72 (2017) (in Russian).
[18] A.R. Yusupov, A.N. Lachinov, L.R. Kalimullina, R.M. Gadiev, D.V. Nikitina. FTT **61**, *3*, 585 (2019) (in Russian).
[19] V.A. Nurmukhamedov, I.A. Chernyshov. Aktual'nye problemy gumanitarnykh i estestvennykh nauk **10-1**, 125 (2015) (in Russian).
[20] S.A. Gridnev, Yu.E. Kalinin, A.V. Sitnikov, O.V. Stogney. Nelinejnye yavleniya v nano- i mikro-geterogennykh sistemakh. Binom. Laboratoriya znanij, M. (2012). p. 352 (in Russian).
[21] V.V. Rylkov, S.N. Nikolaev, K.Yu. Chernoglazov, V.A. Demin, M.Yu. Presnyakov. Phys. Rev. B **95**, 144202 (2017).
[22] Yu.E. Kalinin, A.V. Sitnikov, V.A. Makagonov, V.A. Foshin, M.N. Volochaev. FTT **66**, *11*, 1941 (2024) (in Russian).

[23] V.A. Yuryev, A.G. Chuiko, Yu.E. Kalinin, A.A. Grebennikov, M.A. Kashirin. Neorg. Materialy **60**, *8*, 909 (2024) (in Russian).
[24] L.J. Van der Pauw. Phil. Res. Rep. **13**, *1*, 1 (1958).
[25] A.V. Pashkevich, A.K. Fedotov, Yu.V. Kasyuk, L.A. Bliznyuk, Yu.A. Fedotova, N.A. Basov, A.S. Fedotov, I.A. Svito, E.N. Poddenezhny. Izv. vys. uch. zav. Mat. el. tekhn. **21**, *3*, 133 (2018) (in Russian).
[26] Y. Guo, X.W. Yu, Y.X. Li. J. Appl. Phys. **98**, 053902 (2005).
[27] V.V. Kaminskij, L.N. Vasil'ev, M.V. Romanova, S.M. Solov'ev. FTT **43**, *6*, 997 (2001) (in Russian).
[28] S.V. Vegesna, V.J. Bhat, D. Bürger, J. Dellith, I. Skorupa, O.G. Schmidt, H. Schmidt. Sci. Rep. **10**, 6698 (2020).
[29] W.S. Baer. Phys. Rev. **154**, 785 (1967).
[30] N. Mott, E. Davis. Elektronnye protsessy v nekristallicheskikh veshchestvakh. Mir, M. (1982). T. 1. p. 473 (in Russian).

Translated by A.Akhtyamov